PHOTOCHROMISM OF DOPED BI12SIO20 CRYSTALS

T. V. PANCHENKO 1*, M. P. TRUBITSYN 1,2, V. LAGUTA 2,3

- ¹ Research Institute for Energy Efficient Technologies and Materials Sciences, Oles Honchar Dnipro National University, Science Ave., 72, Dnipro, 49010, Ukraine
- ² Institute of Physics of the Czech Academy of Sciences, Na Slovance 1999/2, 182 00 Prague 8, Czech Republic
- ³ Frantsevich Institute for Problems of Materials Science, NAS Ukraine, Omelyan Pritsak str. 3, Kyiv, 03142, Ukraine
- *Corresponding author: panchtv141@gmail.com

Received: 04.09.2025

Abstract. In the spectral range of 0.5-3.5 eV, both stationary and photoinduced optical absorption, as well as stationary and photoinduced photoconductivity, were studied in $Bi_{12}SiO_{20}$ single crystals doped with nontransition metal ions (Al, Ga, Sn) and transition metal ions (Fe, Cr, Cu, Mn, V, Ag, Mo). It was found that transition metal ions create deep localized centers. In this case, the photochromic effect is controlled by intracenter transitions in those ions whose concentration rises due to photochemical reactions. In crystals doped with non-transition metal ions, the photochromic effect is driven by the redistribution of charge carriers among local levels within the band gap, whose structure is altered by the dopants. In both cases, photoinduced photoconductivity mainly depends on changes in the distribution of carrier recombination currents between fast and slow recombination centers. The possible correlation between the photochromic effect and photoinduced photoconductivity is discussed.

Keywords: Bi₁₂SiO₂₀ doped crystals, absorption spectra, photochromic effect, induced photoconductivity

UDC: 535.33

DOI: 10.3116/16091833/Ukr.J.Phys.Opt.2026.01001

This work is licensed under the Creative Commons Attribution International License (CC BY 4.0).

1. Introduction

Crystals from the sillenite family, $Bi_{12}MO_{20}$ (BMO, where M = Si, Ge, or Ti), display a wide range of functional properties including electro-optic, acousto-optic, magneto-optic, Faraday, and piezoelectric effects, as well as various defect-related phenomena like photorefractive, photochromic, and photogalvanic effects. These properties make sillenite crystals appealing for use in functional electronic devices and optical information processing, such as real-time spatiotemporal light modulation, dynamic holography, and holographic interferometry [1,2].

For such applications, the ability of photorefractive media to reversibly change their refractive index under light exposure is especially important. BMO crystals provide clear advantages over ferroelectrics, including a much faster photorefractive response, and over semiconductors, because of their significantly higher electro-optic coefficients [3,4]. Among sillenites, $Bi_{12}SiO_{20}$ (BSO) crystals stand out for their high photosensitivity ($\sim 10^{-6}$ J×cm⁻²) in the visible spectrum, similar to that of silver-halide materials. During holographic recording in BMO crystals, both photorefractive and non-photorefractive holographic gratings are created; the latter results from the photochromic effect (PhE) [5,6].

Doping is one of the most effective ways to modify the functional properties of BSO crystals, especially their use as holographic media. Although it has been shown that BSO can be doped with various impurities, understanding the effects requires careful analysis of the crystal structure and dopant incorporation models. The BSO unit cell contains two formula

units, made up of oxygen tetrahedra centered by Si⁴⁺ ions and distorted oxygen octahedra coordinated by Bi³⁺ ions [7]. Impurity cations can occupy both Si⁴⁺ and Bi³⁺ sites.

A significant amount of research has explored how various impurities affect the PhE in BSO and $Bi_{12}TiO_{20}$ crystals [8–19]. However, the data available remains scattered because they were obtained under different experimental conditions, often causing inconsistencies in interpretation. Additionally, under certain conditions, other photoinduced photoconductivity (PhI) [20] can develop alongside the PhE. It is reported that holographic recording under PhI conditions is linked to a non-monotonic rise in hologram diffraction efficiency [21]. Furthermore, BSO crystals show complex behavior during hologram recording, fixation, and reading, related to light-induced spatial changes in photoconductivity [22]. Despite this, the exact influence of induced photoconductivity on optical information processing in BMO crystals is still not fully understood, and the connection between photoconductivity and photochromism remains unclear. Currently, studying PhE and induced PhI is highly relevant for optical information processing and various electronic applications [23].

This work aims to thoroughly investigate photoinduced effects, specifically photochromism and photoconductivity, in $Bi_{12}SiO_{20}$ crystals, including both undoped and doped with non-transition and transition metal ions.

2. Experiment

Nominally pure and doped BSO single crystals were grown by the Czochralski method. Doping was performed using non-transition metal ions (Al, Ga, Sn), transition metal ions from the iron group (Cr, Mn, V, Fe, Cu), and from the palladium group (Ag, Mo). The respective dopant oxides were thoroughly mixed with the starting reagents, homogenized by grinding, and synthesized prior to crystal growth. The dopant concentrations in the grown crystals were determined by emission spectral analysis and were found to be (mass %): 6×10^{-2} (Al), 4×10^{-2} (Ga), 1×10^{-1} (Sn), 6×10^{-3} (Cr), 3×10^{-2} (Mn), 5×10^{-2} (V), 3×10^{-2} (Fe), 3×10^{-1} (Cu), 1×10^{-1} (Ag), and 1×10^{-1} (Mo).

Optical absorption and photoconductivity measurements were performed in the photon energy range of hv = 0.5–3.5 eV, limited by the onset of interband and lattice absorption in BSO. Stationary and photoinduced optical transmittance spectra, $t_0(hv)$ and $t^{\rm Ph}(hv)$, respectively, were measured using Cary-5E and Specord M40 spectrophotometers. The measurements were carried out on polished single-crystalline plates with thicknesses ranging from d = 0.03 to 5 mm.

Photoconductivity spectra, both stationary and photoinduced, were obtained using an SPM-2 monochromator with synchronous detection. Stationary photoconductivity was defined as $\Delta \sigma_0^{Ph}(h\nu) = \sigma^{Ph}(h\nu) - \sigma^T$, where $\sigma^{Ph}(h\nu)$ and σ^T represent the conductivities under illumination and in the darkness, respectively. The photoinduced photoconductivity was determined as $\Delta^* \sigma^{Phi}(h\nu) = \Delta \sigma^{Phi}(h\nu) - \Delta \sigma_0^{Ph}(h\nu)$, where $\Delta \sigma^{Phi}(h\nu)$ denotes the photoconductivity after additional photoexcitation.

All measurements were conducted under low illumination using light modulated at 12 Hz in a constant electric field, on samples cut along the (001) crystallographic plane. Silver electrodes were deposited by vacuum evaporation.

The steady-state was defined as the state of the samples after heating to 800 K, followed by slow cooling to room temperature over 24 h. The photoinduced state was prepared by illuminating the crystals with light from a halogen lamp ($h\nu = 2.7 \text{ eV}$, 600 W) for 120 s. Measurements were performed at T = 80 K and 300 K.

The studied spectral characteristics included stationary and photoinduced optical absorption coefficients, $\alpha_0(h\nu)$, $\alpha^{Ph}(h\nu)$; stationary and photoinduced photoconductivity, $\Delta \sigma_0^{\rm ph}(h\nu)$, and $\Delta^* \sigma^{\rm phi}(h\nu)$; additional photochromic absorption, $\Delta \alpha^{\rm phE}(h\nu)$; and normalized additional photoconductivity, $\Delta^{**}\sigma^{\text{PhI}}(h\nu)$. The photochromic effect (PhE) was characterized using the additional absorption spectrum: $\Delta \alpha^{\text{PhE}}(h\nu) = \alpha^{\text{Ph}}(h\nu) - \alpha_0(h\nu)$, and the induced photoconductivity (PhI) evaluated from the normalized was spectrum: $\Delta^{**}\sigma^{PhI}(h\nu) = [\Delta^*\sigma^{Phi}(h\nu) - \Delta\sigma_0^{Ph}(h\nu)]/\Delta\sigma_0^{Ph}(h\nu)$. Optical quenching of both effects was achieved by illuminating the samples with light in the photon energy range hv = 0.7-1.2 eV. The optical absorption coefficient $\alpha(h\nu)$ was calculated from the measured transmittance using the well-known relation:

$$t(h\nu) = \frac{\left(\left(1-R\right)^2 \exp(-\alpha d)\right)}{\left(1-R^2 \exp(-2\alpha d)\right)},\tag{1}$$

where R is the reflection coefficient and d is the sample thickness. Reflection spectra were calculated using: $R(hv) = [(1-n(hv)/(1+n(hv))]^2$, where the refractive index dispersion n(hv) was determined according to:

$$n^2 - 1 = A \left(\frac{\lambda_0^2 \lambda^2}{\lambda^2 - \lambda_0^2} \right) + B \left(\frac{\lambda_1^2 \lambda^2}{\lambda^2 - \lambda_1^2} \right), \tag{2}$$

with the following parameters for BSO: $A = 92.22 \,\mu\text{m}^{-2}$, $B = 0.534 \,\mu\text{m}^{-2}$, $\lambda_0 = 0.22 \,\mu\text{m}$, $\lambda_1 = 0.378 \,\mu\text{m}$, $\lambda = 1/\nu$ [24].

The probability of substituting Si⁴⁺ or Bi³⁺ with a specific impurity ion was estimated using the mixing energy approach and the isomorphism energy ratio.

$$Q = b(\Delta r / R_m)^2 + (\Delta s)^2, \tag{3}$$

where Q is the mixing energy, b is a constant specific to the matrix, Δr is the difference in ionic radii between the dopant and the host cation, and R_m is the average bond length in the corresponding oxygen polyhedron (Si–O or Bi–O). The term $\Delta s = s_1 - s_2$ represents the difference in the ionicity degrees of the cation–oxygen bonds, where: $s_1 = (\chi_1 - \chi_0)/(\chi_1 + \chi_0)$, $s_2 = (\chi_2 - \chi_0)/(\chi_2 + \chi_0)$, and χ_0 is the electron affinity energy of the host cations (Si⁴⁺, Bi³⁺), while χ_1 and χ_2 correspond to the impurity ions substituting Si⁴⁺ or Bi³⁺, respectively.

3. Results and Discussion

3.1. Optical Absorption

The steady-state and photoinduced optical absorption spectra of the investigated BSO crystals are shown in Fig. 1. Two distinct photon energy ranges are identifiable: region A (3.5–2.0 eV) and region B (2.0–0.5 eV).

3.1.1. Undoped BSO crystals. In region A, the spectra $\ln(\alpha_0(h\nu))$ and $\ln(\alpha^{\rm Ph}(h\nu))$ of undoped BSO crystals show a clear absorption shoulder (the interval 2.3–3.0 eV, Fig. 1a–j, curves 1, 1'). This feature is usually linked to the presence of intrinsic defects. The main defects are antisite BiSi³⁺ and BiSi⁵⁺ ions, which replace Si⁴⁺ ions in oxygen tetrahedra. These ions act as donors and acceptors, creating local levels within the forbidden zone. This aligns with earlier reports on unalloyed sillenite crystals [9]. Absorption in the B region is weak. Photoinduced absorption significantly exceeds stationary absorption within the energy range of 1.0–3.0 eV. The $\ln(\alpha^{\rm Ph}(h\nu))$ spectrum shows broad peaks in the A region, with peak energies at roughly $h\nu_{\rm max} \approx 2.05$ eV and 2.75 eV (Fig. 1a–j, curves 1'). This suggests an increase in the concentration of BiSi³⁺ or BiSi⁵⁺ ions due to a photochemical reaction.

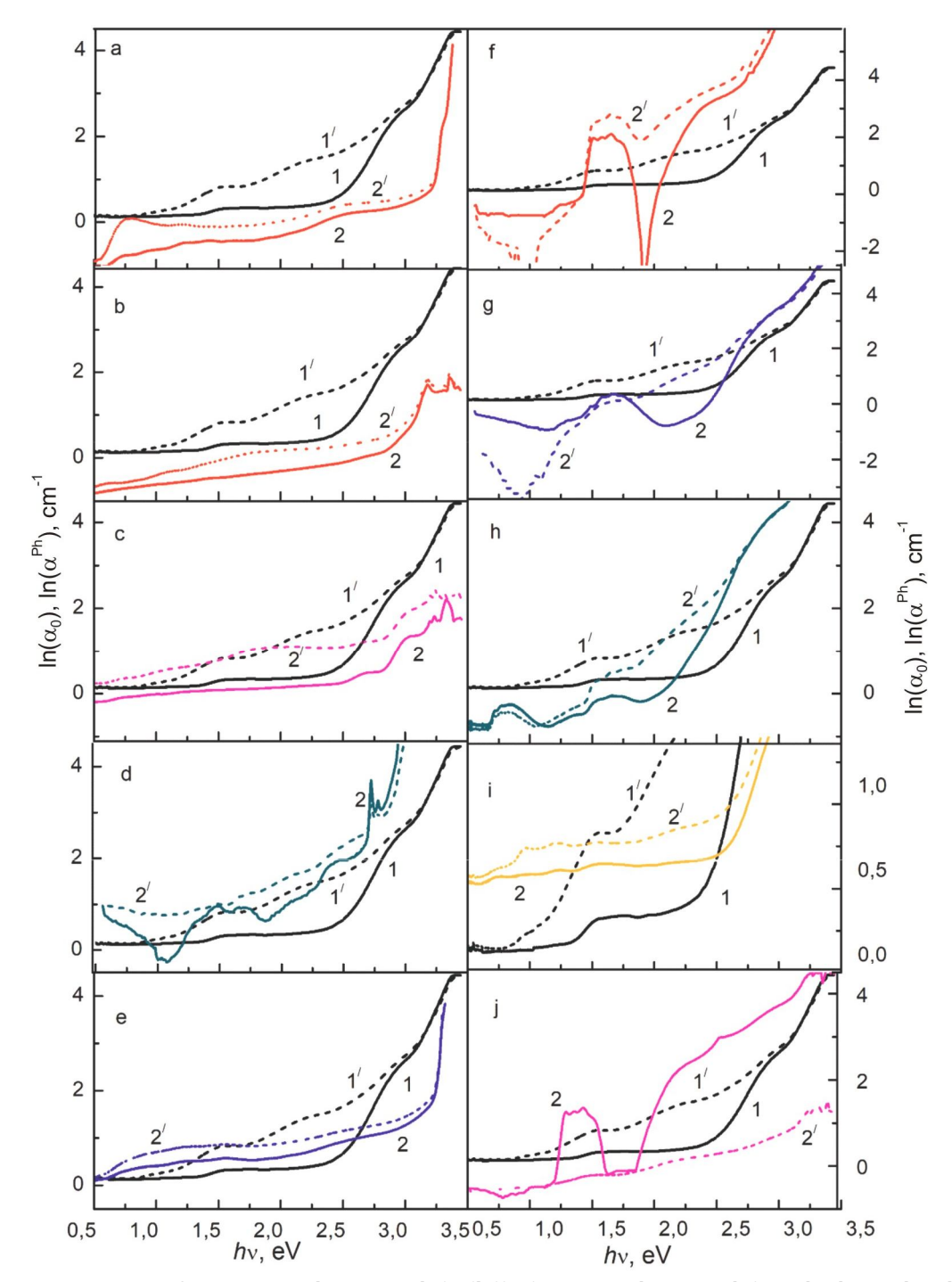


Fig. 1. Spectra of stationary absorption $\ln(\alpha_0(hv))$ (curves without stroke) and photoinduced absorption $\ln(\alpha^{\text{ph}}(hv))$ (dashed curves with stroke/) of undoped (curves 1, 1') and doped (curves 2, 2') BSO crystals with: Al (a); Sn (b); Mo (c); Fe (d); Ga (e); Cr (f); Mn (g); Cu (h); Ag (i); V (j). T = 80 K.

3.1.2. BSO crystals doped with Al, Ga, Sn. Non-transition metal ions such as Al³+, Ga³+, Sn⁴+, and Sn²+ have charge states with the electron configurations $3s^23p^1$ (Al), $4s^24p^1$ (Ga), $5s^25p^2$ (Sn²+), and $5s^25p^0$ (Sn⁴+). In BSO crystals, these ions cause a reduction in steady-state optical absorption throughout the entire spectral range, along with a weakening of the absorption

shoulder in the A region (Fig. 1a, b, e, curves 2). This can be explained if Al, Ga, and Sn ions substitute for defects – namely antisite BiSi₃₊ and BiSi⁵⁺ – which occupy Si⁴⁺ lattice sites and are responsible for the absorption shoulder in undoped BSO. Therefore, Al³⁺, Ga³⁺, and Sn²⁺ ions are localized at oxygen tetrahedra, replacing Si⁴⁺ ions, and act as acceptors. The exact role of Sn⁴⁺ ions still needs clarification. The acceptor behavior of Al³⁺ ions is supported by studies of the electrical conductivity of BSO:Al crystals [24].

The observed decrease in steady-state optical absorption is attributed to the redistribution of electrons to deeper localized forbidden states associated with Al^{3+} , Ga^{3+} , Sn^{2+} , and possibly Sn^{4+} centers.

Photoinduced optical absorption, $\alpha^{\rm Ph}(h\nu)$, slightly exceeds the steady-state absorption in BSO:Al and BSO:Ga crystals, while Sn ions cause a much more significant increase in absorption. A key feature of the $\ln \alpha^{\rm Ph}(h\nu)$ spectra is the presence of absorption bands at photon energies $h\nu<1$ eV (Fig. 1a, b, e, curves 2'). The maximum points of these bands are systematically shifted toward the infrared region, from $h\nu_{\rm max}=0.79$ eV (Al) to $h\nu_{\rm max}=0.56$ eV (Sn), which correlates with the increase in the electron shell diameter and the decrease in the ionization potential of Sn ions [10].

In BSO:Al crystals, paramagnetic centers are generated upon photoexcitation. These centers were identified using magnetic circular dichroism (MCD) and optically detected paramagnetic resonance (ODPR) techniques [25]. In the ground state, Al^{3+} ions substitute for Si^{4+} ions in oxygen tetrahedra with T_d symmetry. In this configuration, Al^{3+} exists as the diamagnetic complex $[AlSiO_4]^-$. Upon photoexcitation, an O^- hole center (configuration $1s^22s^22p^5$) and an additional positive charge – a hole (h) – are formed. The O^- ion can be regarded as a paramagnetic center due to the presence of unpaired electrons that give rise to a magnetic moment. The hole is delocalized, at least over the oxygen atoms forming the tetrahedral framework. Then the complex: Al^{3+} ion, O^- center, and h hole can be represented as $[Al_{si}O_4]^- + h$. The existence of the hole is confirmed by a Landé factor value exceeding 2 [25]. Paramagnetism manifests itself because aluminum participates in complexes containing unpaired electrons.

When excited within the fundamental optical absorption band ($hv_1 = 3.3-3.5 \text{ eV}$) and the adjacent interval ($hv_2 = 2.8-2.9 \text{ eV}$) in undoped and Al, Ga, Sn-doped BSO crystals, broad photoluminescence bands are observed in the ranges $hv_3 = 1.7-2.7 \text{ eV}$ and $hv_4 = 1.0-1.5 \text{ eV}$. The photoluminescence is attributed to radiative recombination processes, which are determined by electron transitions "impurity level \leftrightarrow conduction band" [26]. The influence of Ga and Sn ions on both steady-state and photoinduced optical absorption, as well as on the photoluminescence of BSO crystals, is similar to that of Al ions. This similarity suggests that their photoionization processes follow the same mechanism.

Note that increasing the temperature from 80 to 300 K causes a reduction in photo-induced absorption in the $\ln(\alpha^{ph}(h\nu))$ spectra of BSO crystals doped with non-transition metal ions.

3.1.3. BSO crystals doped with transition metal ions. Doping with transition metal ions from the iron group (Fe, Cr, Mn, Cu) and the palladium group (Mo, Ag) results in the appearance of distinct absorption bands in both the A and B regions of the steady-state and photoinduced absorption spectra (Fig. 1c, d, f–j, curves 2, 2'). These bands are attributed to d-d electronic transitions and charge-transfer transitions characteristic of each dopant element. They

overlap with the intrinsic absorption shoulder, leading either to an increase in its intensity (Fe, Cr, Mn, Cu, Ag; Fig. 1d, f–i, curves 2, 2') or to a decrease in its intensity (V, Mo; Fig. 1c, j, curves 2, 2'). Photoinduced absorption exceeds steady-state absorption in the A region for Cr-, Mn-, and Cu-doped crystals, and in both the A and B regions for Ag-, Mo-, and Fe-doped crystals. A distinctive feature of the $\ln(\alpha^{\text{Ph}}(h\nu))$ spectra of BSO crystals doped with Cr, Mn, Cu, or V ions is a reduction in absorption in the B region (Cr, Mn, Cu) or in both the A and B regions (V; Fig. 1f–h, j, curves 2').

In previous studies, using optical spectroscopy, crystal field theory, magnetic circular dichroism (MCD), and optically detected paramagnetic resonance (ODPR), and taking into account the mixing energy Q, the charge states and localization of the transition metal ions in the BSO crystal lattice were determined [8, 17–19, 27, 28].

Cr, Mn, and V ions. In the $\ln(\alpha_0(hv))$ spectra of BSO:Cr, BSO:Mn, and BSO:V crystals, Cr, Mn, and V ions give rise to three intense absorption bands in the energy intervals hv = 1.1 - 1.8, 1.6 – 2.9, and 2.9 – 3.4 eV (Fig. 1f, g, j, curves 2). These bands are attributed to intracenter d–d electronic transitions: ${}^4A_{2g}({}^4F) \rightarrow {}^4T_{2g}({}^4F)$, ${}^4A_{2g} \rightarrow {}^4T_1({}^4F)$ and ${}^4A_{2g} \rightarrow {}^4T_1({}^4P)$ in ions with the 3d³ electronic configuration: Cr³+, Mn⁴+, and V²+, which substitute for Bi³+ ions in oxygen octahedra (coordination number, (c. n.) 6) [27, 28]. A characteristic feature of the spectra is the Π -shaped profile of the absorption bands in the $hv = 1.1-1.8 \, \text{eV}$ range. The main components of these Π -shaped bands are located at $h\nu_{\text{max}} = 1.69 \text{ eV}$ (BSO:Mn) and $h\nu_{\rm max} = 1.16$ eV (BSO:V), and are shifted relative to the $h\nu_{\rm max} = 1.65$ eV (BSO:Cr) component toward the short-wavelength and long-wavelength regions, respectively. Similar displacements are described in the literature, for example, for V²⁺, Cr³⁺, and Mn⁴⁺ ions with a c. n. 6 in MgO and Al_2O_3 crystals. According to crystal field theory [29], these shifts reflect an increase (Mn⁴⁺) or decrease (V²⁺) in the ionic charge state relative to Cr^{3+} . The $h\nu_{max}$ values determine the strength of the crystal field, calculated as $Dq = 0.1 \times hv_{\text{max}}$. These values are relatively small for a $3d^3$ configuration with c.n. 6; for example, in laser oxide crystals containing Cr^{3+} , $Dq \approx 0.20$ –0.22 eV. However, they are consistent with the empirical relationship $Dq \sim 1/R^5$, where R is the distance between the metal and oxygen ions in the octahedra of BSO crystals [27]. In Bi₁₂SiO₂₀ crystals with Cr ions, broad photoluminescence bands were observed in the same ranges as the optical absorption bands: hv = 1.1-1.8 and 1.6–2.9 eV [30]. They can be attributed to transitions from excited states to the ground state: ${}^{4}T_{2g}({}^{4}F) \rightarrow {}^{4}A_{2g}({}^{4}F)$ and ${}^{4}T_{1}({}^{4}F) \rightarrow {}^{4}A_{2g}({}^{4}F)$.

For V ions, the situation may be complicated. It is shown in the literature that when the V^{2+} ion is in the octahedral oxygen coordination the electron transition ${}^4A_2(F) \rightarrow {}^4T_2(F)$ observes at 1.47 eV and 1.54 eV. The other two electron transitions at 1.8 eV and 1.86 eV correspond to the V^{3+} ions in the bismuth position for different materials [15, 31, 32].

Photoinduced absorption exceeds steady-state absorption in region A for crystals doped with Cr and Mn. A distinctive feature of the $\ln(\alpha^{\rm Ph}(h\nu))$ spectra of BSO crystals doped with Cr and Mn ions is the disappearance of the absorption band in the $h\nu=0.5-1.5$ eV range. This behavior indicates a change in the relative concentrations of ions in the ${\rm Cr^{3+}/Cr^{2+}}$ and ${\rm Mn^{4+}/Mn^{3+}}$ pairs as a result of photochemical reactions, favoring the formation of ${\rm Cr^{3+}}$ and ${\rm Mn^{4+}}$ ions, which dominate in the steady state of BSO:Cr and BSO:Mn crystals. In crystals doped with V, absorption decreases across the entire spectral range (Fig. 1f, g, j, curves 2'). In contrast, this behavior indicates a decrease in the concentration of the dominant ${\rm V^{3+}}$ and ${\rm V^{2+}}$

ions [27, 28]. Further research is required to elucidate the mechanism of the photochemical reactions in BSO:V crystals.

Cu and Ag ions. In the $\ln(\alpha_0(h\nu))$ spectra of BSO:Cu crystals, Cu ions give rise to well-defined absorption bands in the intervals $h\nu=0.73-1.50$, 1.48-1.65, 2.66-2.79, and 3.10-3.23 eV (Fig. 1h, curves 2). The number and spectral positions of these bands allow their attribution to d-d transitions: ${}^3A_{2g} \rightarrow {}^3T_{2g}$, ${}^3A_{2g} \rightarrow {}^3T_{1g}$, ${}^3A_2 \rightarrow {}^1E_{1g}$ in Cu³⁺ ions (3d⁸ configuration, c.n.6), which substitute for Bi³⁺ ions in oxygen octahedra [17,19]. A distinctive feature of both the $\alpha_0(h\nu)$ and $\alpha^{\text{Ph}}(h\nu)$ spectra is the "comb-like" structure formed by four narrow bands of similar intensity in the $h\nu=1.48-1.65$ eV range (Fig. 1h, curves 2, 2'). This structure arises from the splitting of the absorption band due to the reduction in local symmetry of the oxygen octahedra in BSO to C_{2 ν}.

The band near the fundamental absorption edge at $hv = 3.1 - 3.23 \, \text{eV}$ is attributed to a ligand-to-metal (L-M) charge transfer transition. For isolated CuO₆ octahedra, this transition typically occurs in the UV region ($hv >> 3.7 \, \text{eV}$). However, it shifts to lower photon energies when CuO₆ octahedra form clusters or associate, indicating interaction between adjacent polyhedra. The presence of Cu²⁺ ions (3d⁹ configuration) with a c n. 6 is also suggested, contributing a broad absorption band in the $hv = 0.5 - 1.5 \, \text{eV}$ region, d-d transitions ${}^2E_g({}^3D) \rightarrow {}^2T_{2g}({}^3D)$ [17,19].

In the $\ln(\alpha^{Ph}(h\nu))$ spectra, the intensity of the band associated with Cu^{2+} ions decreases, while the intensities of the other bands increase (Fig. 1h, curve 2'). This behavior indicates a decrease in the concentration of Cu^{2+} ions accompanied by a corresponding increase in the concentration of Cu^{3+} ions during photoionization.

In the $\ln(\alpha_0(h\nu))$ spectra of BSO:Ag crystals, three narrow absorption bands are observed in the near-infrared region at $h\nu_{max}=0.97$, 1.19, and 1.39 eV (Fig. 1i, curve 2). These bands are attributed to d–d transitions in Ag^{2+} ions (4d 9 configuration, c. n. 6) substituting for Bi^{3+} ions in oxygen octahedra [17]. The energy-level diagram is analogous to that for Cu^{2+} ions; however, the splitting of the 2E_g state into $^2A_{1g}$ and $^2B_{1g}$, and of the $^2T_{2g}$ state into $^2B_{2g}$ and 2E_g , is more pronounced. The components of the absorption band can thus be assigned to the following electron transitions: $^2B_{1g} \rightarrow ^2A_{1g}$ (0.97 eV), and $^2B_{1g} \rightarrow ^2B_{2g}$ (1.19 eV), and $^2B_{2g} \rightarrow ^2E_g$ (1.39 eV). In the $\ln(\alpha^{ph}(h\nu))$ spectra, the intensity of these bands increases (Fig. 1i, curve 2'). We also assume that a certain fraction of Ag^+ ions (4d 10 configuration, c. n. 6) is present. These ions are optically inactive, since the Ag^+ ground state does not split in the crystal field. However, upon photoexcitation, Ag^+ ions can be oxidized to Ag^{2+} .

Fe ions. A typical feature of the $\ln(\alpha_0(h\nu))$ spectra of BSO:Fe crystals is a doublet of absorption bands in the range $h\nu=2.72$ –2.74 eV (Fig. 1d, curve 2). According to electron paramagnetic resonance (EPR) spectroscopy data [33], these bands are linked to electronic transitions in Fe³⁺ ions (3d⁵ configuration, c.n.4), which substitute for Si⁴⁺ ions in oxygen tetrahedra. As a result, the absorption bands at $h\nu=1.0$ –2.0 eV and 2.40–2.64 eV (Fig. 1d, curve 2), along with the doublet, are ascribed to the following electronic transitions: $^6A_1(^6S) \rightarrow ^4T_1(^4G)$, $^6A_1(^6S) \rightarrow ^4T_2(^4G)$, and $^6A_1(^6S) \rightarrow ^4A_1g$, $^4E_2g(^4G)$. The broad band at $h\nu=2.76$ –3.34 eV is assigned to a ligand-to-metal (L–M) charge-transfer transition of the type O^2 – → Fe³⁺ [19]. We also observe an absorption band in the infrared region at $h\nu=0.5$ –1.0 eV (Fig. 1d, curve 2), indicating the presence of Fe²⁺ ions (3d⁶ configuration, c.n. 4). This band corresponds to a single spin-allowed transition $^5E(^5D) \rightarrow ^5T_2(^5D)$, while the other spin-forbidden transitions produce weak absorption bands in the visible region.

In the $\ln(\alpha^{Ph}(h\nu))$ spectra, the intensities of the doublet and the L-M charge-transfer

band decrease, indicating a reduction in the concentration of Fe^{3+} ions. In contrast, the intensities of the other bands increase, reflecting a corresponding rise in the concentration of Fe^{2+} ions under photoexcitation (Fig. 1d, curve 2') [19].

Mo ions. In the $\ln(\alpha_0(h\nu))$ and $\ln(\alpha^{\rm Ph}(h\nu))$ spectra of BSO:Mo crystals, the absorption bands are associated with intracenter d-d transitions in Mo⁵⁺ ions (4d¹ configuration, c.n.4). Short-wavelength ligand-to-metal (*L-M*) charge transfer bands appear at $h\nu_{\rm max}$ = 2.78 and 3.26 eV (Fig. 1c, curve 2), which are characteristic of Mo⁵⁺ ions. A certain fraction of optically inactive Mo⁶⁺ ions (4d⁰ configuration) occupying oxygen tetrahedra might also be present. In the $\ln(\alpha^{\rm Ph}(h\nu))$ spectra, the intensities of the photoinduced absorption bands increase (Fig. 1c, curve 2'), which is due to the reduction of Mo⁶⁺ ions to Mo⁵⁺ under photoexcitation [18]. This interpretation is further supported by independent experimental data [11].

It should be noted that the $\alpha_0(h\nu)$ and $\alpha^{\rm Ph}(h\nu)$ spectra of BSO crystals doped with transition metal ions exhibit only minor changes as the temperature increases from 80 to 300 K. However, at temperatures T > 300 K, the optical absorption of BSO:Mn and BSO:Cr crystals undergoes significant variations [34].

3.2. Photoconductivity

The steady-state and photoinduced photoconductivity spectra of the investigated BSO crystals are shown in Fig. 2. The spectral shape and the magnitude of photoconductivity vary significantly with doping and temperature.

At T=300 K, the spectra of $\ln(\Delta\sigma_0^{\rm Ph}(h\nu))$ and $\ln(\Delta^*\sigma^{\rm Phi}(h\nu))$ for undoped BSO crystals exhibit a pronounced broad peak in region A (Fig. 2a–e, curves 1, 1'). This feature is missing in crystals doped with Al, Cr, or Cu (Fig. 2a, b, d, curves 2, 2'). A clear threshold-like rise in photoconductivity appears in region B for all samples. Doped crystals have lower steady-state photoconductivity compared to undoped ones (Fig. 2a–e, curves 2). In Al- and Cu-doped crystals, the induced photoconductivity surpasses the steady-state value throughout the entire spectral range (Fig. 2a, e, curves 2'). For undoped BSO and crystals doped with Cr, Mn, or Ag ions, this excess occurs only within the A band, near the fundamental absorption edge at photon energies $h\nu > 2.3$ eV (Fig. 2a–c, j, curves 2').

The spectra $\Delta \sigma_0^{\rm Ph}(h\nu)$ and $\Delta^* \sigma^{\rm Phi}(h\nu)$ show peaks of different intensities, along with regions (thresholds) marked by a sharp rise in photoconductivity. This spectral behavior is typical for semiconductors, where photoconductivity results from the depletion of localized impurity levels within the forbidden gap. The spectral positions of the photoconductivity maxima in the $\Delta \sigma_0^{\rm Ph}(h\nu)$ spectra enable an estimation of the optical activation energy (0E_a) of these levels (Table 1).

Table 1. Optical activation energy ${}^{0}E_{a}$ of local levels of the forbidden gap in BSO crystals. T = 300 K.

Crystal		⁰ E _a , eV										
BSO	0.79	1.02		1.5	1.92	2.22	2.45	2.6	2.86	3.03	3.2	
BSO:Al	0.84			1.52		2.2	2.45	2.6		3.0	3.19	3.39
BSO:Ga	0.86			1.52		2.2	2.45	2.6			3.13	
BSO:Mn	0.84	1.0	1.36	1.52	1.92	2.18	2.48	2.55		3.04		
BSO:Cr	0.74	1.15	1.37	1.48	1.93		2.45	2.55	2.87	3.02	3.26	
BSO:Cu	0.72	0.83	1.25	1.5	1.9	2.26		2.52	2.89	3.02	3.23	
BSO:V	0.86	1.0	1.32	1.52	1.89				2.8	3.02	3.27	

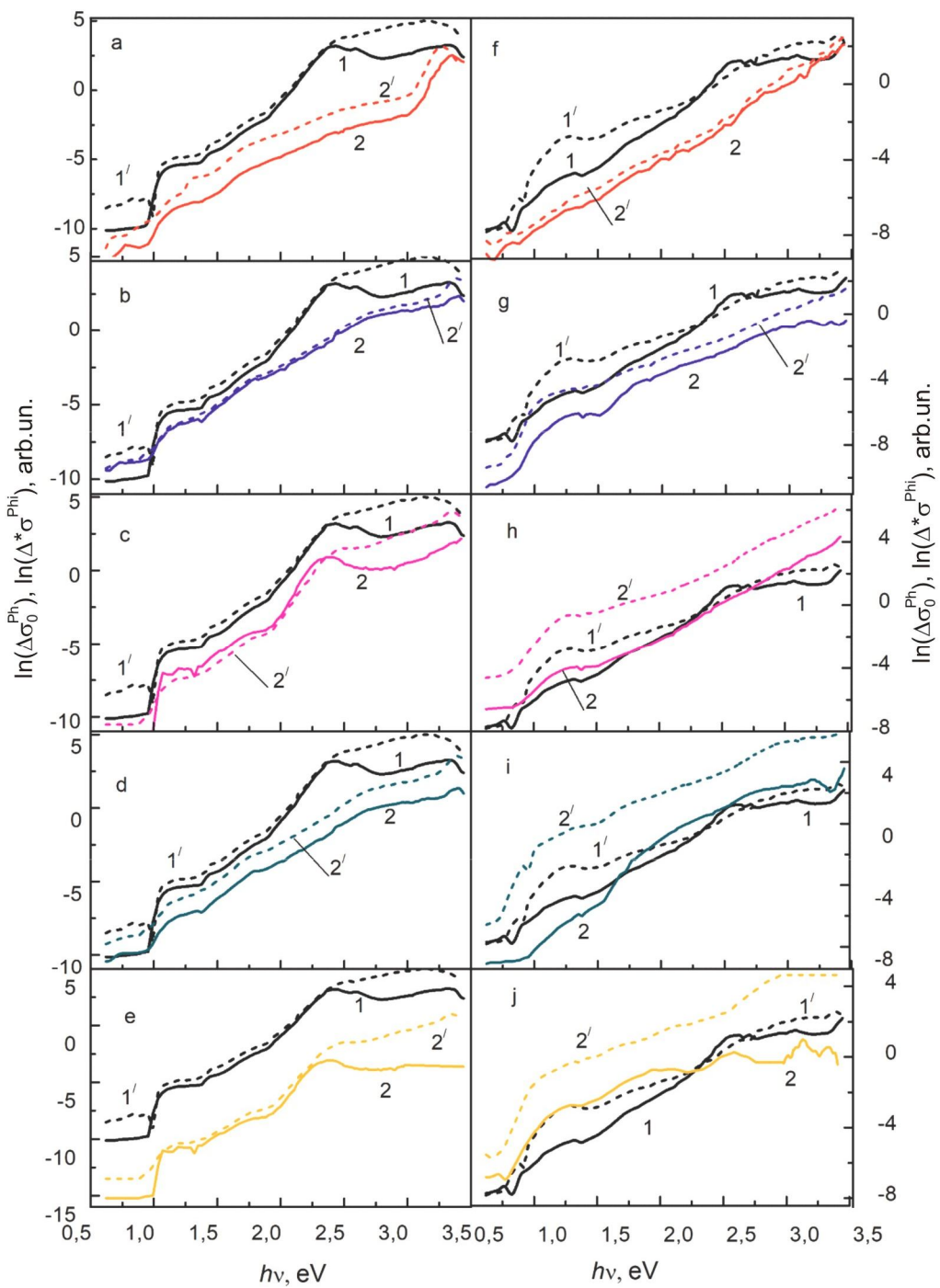


Fig. 2. Spectra of steady-state photoconductivity $\ln(\Delta\sigma_0^{\rm Ph}(h\nu))$ (curves without stroke) and photo induced photoconductivity $\ln(\Delta^*\sigma^{\rm Phi}(h\nu))$ (dashed curves with stroke/) of undoped (Fig. 2a – j, curves 1, 1') and doped (Fig. 2a – j, curves 2, 2') BSO crystals with: Al (a, f); Cr (b, g); Mn (c, h); Cu (d, i); Ag (e, j). at T=300 K (a, b, c, d, e) and 80 K (f, g, h, i, j).

It was found that all crystals possess a photoactive level with ${}^{0}E_{a} \approx 0.80$ –0.86 eV. The incorporation of Al and Ga ions leads to the depletion of levels characteristic of undoped BSO due to the occupation of deep acceptor states with optical ionization energies ${}^{0}E_{a}$ = 3.0 and

3.39 eV (Table 1). As a result, both photoconductivity and optical absorption decrease in the A and B spectral regions, accompanied by the disappearance of the absorption shoulder and the broad photoconductivity peak in region A (Fig. 1a, e, curves 2; Fig. 2a, curve 2). The Mn, Cr, Cu, and V ions do not significantly alter the level structure of undoped BSO but introduce an additional level with ${}^{0}E_{a} = 1.25$ -1.32 eV (Table 1, Figs. 2f, g, h, j). Probably, the appearance of these levels is due to the delocalization of some energy states involved in intra-center electron transitions in Cr, Mn, Cu, and V ions. The induced photoconductivity of all crystals differs from the stationary one by a significant increase near the edge of the fundamental optical absorption (A-range, Fig. 2a – j, curves 2').

At T=80 K, the spectra $\ln(\Delta\sigma_0^{\rm Ph}(h\nu))$ (Fig. 2f-j, curves 1, 2) and $\ln(\Delta^*\sigma^{\rm Phi}(h\nu))$ (Fig. 2f-j, curves 1', 2') undergo significant transformation, characterized by an increase in photoconductivity in the B region ($h\nu$ < 2.3 eV) and a corresponding decrease in the A region ($h\nu$ > 2.3 eV). Concurrently, the effect of induced photoconductivity becomes more pronounced for all crystals except BSO:Al (Fig. 2f, curve 2'), as seen in Fig. 2f – j (curves 1', 2').

Previous studies of the temperature dependence of the steady-state photoconductivity of undoped and doped BSO crystals have shown that charge carrier transport is accompanied by multi-center recombination. This causes temperature-dependent activation or suppression of the photocurrent [35,36]. Both effects result from the switching of electron recombination currents. If switching occurs from s-centers of fast recombination to r-centers of slow recombination, activation of the photocurrent is observed; if the switching occurs in opposite direction, the photocurrent is quenched. A decrease in photoconductivity at T= 80 K demonstrates its quenching. The effect of temperature on induced photoconductivity is also determined by these effects, but differently for different impurities. At 300 K, induced photoconductivity is greater in BSO, BSO with Al, Ag crystals (Fig. 2a, i, curves 1', 2'), and at 80 K, it is greater in BGO with Mn, Cu, and Ag crystals (Fig. 2g, h, i, curves 2').

3.3. Photochromic effect and photoinduced photoconductivity

The spectra $\Delta\alpha^{\rm PhE}(h\nu)$ and $\Delta^{**}\sigma^{\rm PhI}(h\nu)$, characterizing the PhE and PhI effects, respectively, turn out to be significantly different (Fig. 3). In the $\Delta\alpha^{\rm PhE}(h\nu)$ spectra, the PhE bands that form their structure are located in the middle of the studied spectral range (Fig. 3a, b). The $\Delta^{**}\sigma^{\rm PhI}(h\nu)$ spectra are dominated by bands adjacent to the edge of the fundamental optical absorption and the infrared edge of the studied range (Fig. 3c, d).

The PhI $\Delta^{**}\sigma^{\text{PhI}}$ (hv) spectra are normalized relative to the stationary photoconductivity $\Delta\sigma_0^{\text{Ph}}(hv)$ of the studied crystals. They represent the distribution of energy level densities within the forbidden zone, which are filled with charge carriers during the photoexcitation of crystals by photons with an energy of hv = 2.7 eV. Taking into account the mixed (electron-hole) type of photoconductivity, it can be assumed that the values of $\Delta^{**}\sigma^{\text{PhI}}(hv)$ correlate with the filling of energy levels by charge carriers.

In undoped BSO and BSO with Al and Mo ions, intense IR bands of PhI spectra are observed (Fig. 3c, curves 1–3). This indicates a high concentration of small levels near the edges of the conduction band and valence band. In the crystals BSO with Al, the spectral positions of the PhI strip correspond to the positions of the PhE stripes (Fig. 3a, c, curves 1). In BSO crystals with Cu and Cr ions, the most intense broad structured bands of the PhI spectra are observed, occupying the B region (Fig. 3d, curves 1–3), with Mn present. However, the photochromic effect in the B region is weakened (Fig. 3b, curves 1–3). These

ions increase the concentration of local levels filled with charge carriers and occupying the lower half of the band gap (Fig. 3d, curves 1-3). It should be noted that photoexcitation also causes electrons to fill deep levels with optical activation energy OEa > 2.5 eV (Fig. 3c, curves 2.3; Fig. 3d, curves 1-3).

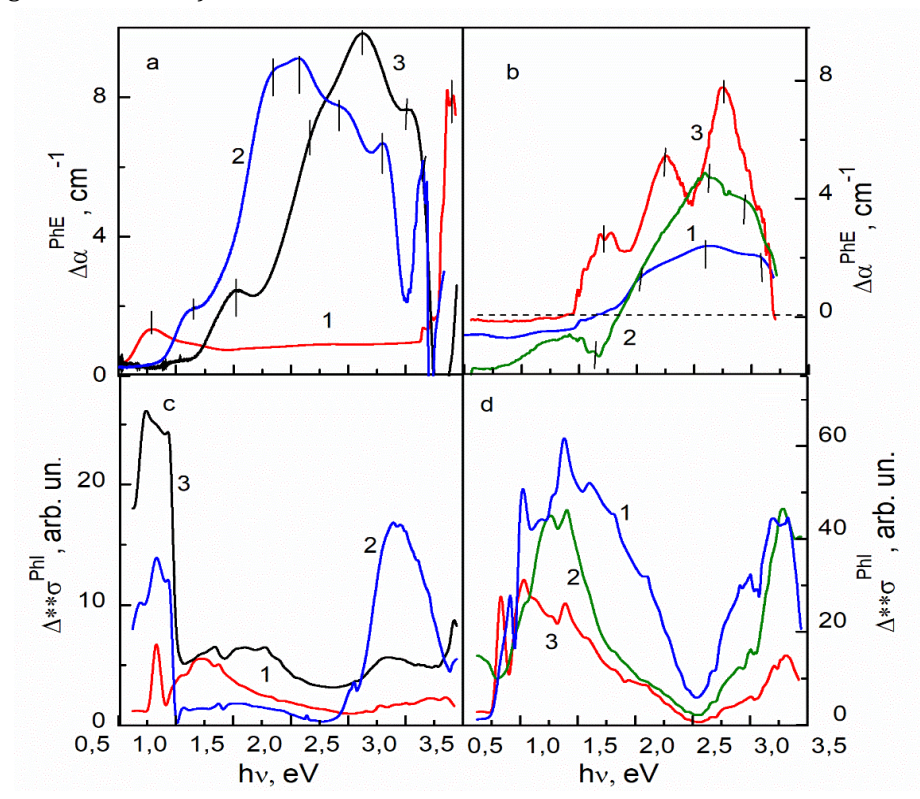


Fig. 3. PhE spectra $\Delta \alpha^{\text{PhE}}(h\nu)$ (Fig. 3a, b) of the crystals BSO with Al, Mo and undoped BSO (Fig. 3a, curves 1 – 3), of the crystals BSO with Cu, Mn, Cr (Fig. 3b, curves 1 – 3); PhI spectra $\Delta^{**}\sigma^{\text{PhI}}(h\nu)$ (Fig. 3c, d) of the crystals BSO with Al, Mo and undoped BSO (Fig. 3c, curves 1 – 3), of the crystals BSO with Cu, Mn, Cr (Fig. 3d, curves 1 – 3). T = 80 K.

The difference in the energy positions of the main bands in the $\Delta\alpha^{\text{PhE}}(h\nu)$ and $\Delta^{**}\sigma^{\text{PhI}}(h\nu)$ spectra mainly indicates that there is no direct link between the PhE and PhI effects.

In the crystals doped by the ions of transition metals, the PhE is due to the change in the ratio between the concentrations of the same ions, but with different charge states.

Changes occur as a result of photochemical reactions according to the following schemes: $Cr^{2+} - e \rightarrow Cr^{3+}$, $Mn^{4+} + e \rightarrow Mn^{3+}$, $V^{2+} + e \rightarrow V^{3+}$; $Cu^{3+} + e \rightarrow Cu^{2+}$, $Fe^{3+} + e \rightarrow Fe^{2+}$, $Ag^+ - e \rightarrow Ag^{2+}$, $Mo^{5+} + e \rightarrow Mo^{4+}$, $Mo^{6+} + e \rightarrow Mo^{5+}$ [8, 17 – 19, 27, 28].

The main absorption bands in the $\Delta \alpha^{\rm Ph} E(h \nu)$ spectra are due to intra-center electronic transitions within these ions (see Section 3.2). Importantly, the spectral positions of the main bands in the PhE spectra do not match those in the $\Delta^{**}\sigma^{\rm Ph} I(h \nu)$ spectra, that is, the energy levels within the bandgap that become occupied during photoinduced photoconductivity (Fig. 3a, c, curves 2; and Fig. 3b, d, curves 1–3).

These findings indicate that transition metal ions introduce deep localized centers in BSO crystals. These centers are characterized by strong electron–phonon coupling, as

supported by the data presented in [27]. It is also well established that deep centers can form complexes with ions from the first and second coordination spheres, as well as with intrinsic lattice defects. This explains the observed differences in the spectral positions of the $\Delta^{**}\sigma^{\text{PhI}}(h\nu)$ bands for Mo ions substituting Si in oxygen tetrahedra, compared to Cr, Mn, V, and Cu ions substituting Bi in oxygen octahedra (Fig. 3c, curve 2; and Fig. 3d, curves 1–3). Moreover, this accounts for the appearance of a new energy level with an activation energy of approximately ${}^{0}E_{a} \approx 1.3$ eV in the bandgap of BSO crystals doped with Cr, Mn, V, or Cu ions (Table 1).

Non-transition metals doping ions Al, Ga, Sn create acceptor levels. In the undoped BSO, antisite ion Bi⁵⁺ or Bi³⁺ creates donor or acceptor levels. Under photoexcitation, the charge of donors and acceptors changes due to the capture of holes h or electrons e: Al⁽⁰⁾ + $h \rightarrow$ Al⁽⁺⁾, Ga⁽⁰⁾ + $h \rightarrow$ Ga⁽⁺⁾, Sn⁽⁰⁾ + $e \rightarrow$ Sn⁽⁻⁾, Bi⁽⁰⁾ + $h \rightarrow$ Bi⁽⁺⁾, and Bi⁽²⁺⁾ + $2e \rightarrow$ Bi⁽⁰⁾. Here, the superscript in brackets indicates a change in the charge of the acceptor or donor from neutral (0) to positive (+) or negative (-) [10]. In this case, there is an incomplete correlation between the spectra $\Delta \alpha^{\text{PhE}}(h\nu)$ and $\Delta^{**}\sigma^{\text{PhI}}(h\nu)$ (Fig. 3a, curve 1, and Fig. 3c, curve 1).

The photoconductivity is caused by photoinduced filling of energy levels near the bottom of the conduction band and shallow levels near the top of the valence band. These levels form tails of states near the mentioned bands. A common feature of the photoconductivity and the photochromic effect is that both effects are excited by light with $hv \ge 2.7$ eV.

The practically significant characteristics of the photochromic effect include the integral

photochromic efficiency
$$\Psi$$
, defined as: $\int_{hv_1}^{hv_2} \Delta \alpha^{\text{PhE}} hv \, dhv$, where hv_1 and hv_2 are the

boundaries of the spectral range of the PhE, and $\Delta \alpha^{\rm PhE}(h\nu)$ is the change in absorption due to the photochromic transformation. Another important parameter is the reversibility (or reproducibility) coefficient K, which is defined as the ratio Ψ_1/Ψ_2 for two consecutive "photo induced – optical bleaching" cycles. Additional key parameters include the spectral width of the PhE $\Delta h\nu = h\nu_2 - h\nu_1$, as well as the spectral positions of the maxima $h\nu_{\rm max}$ of the intense PhE bands characteristic of the specific type of doping ions. For the studied crystals exhibiting a significant PhE, the corresponding characteristics are summarized in Table 2.

Table 2. C	haracteristics	of Ph	E in und	loped	and o	doped	BSO	crystals	s*

Crystal	Ψ, eV·cm ⁻¹	K	$\Delta h \nu$, eV	$h u_{ m max}$, eV
BSO	10.5	0.93	1.5 - 3.25	1.52, 2.19, 2.62, 3.05
BSO:Ga	1.75	0.2	0.74 - 3.3	0.96, 2.19, 3.09
BSO:Al	0.3	0.15	0.5 - 1.25	0.77, 3.32
BSO:Sn	3.72	0.7	0.6 - 3.38	0.63, 1.86, 2.83, 3.16
BSO:Cr	6.52	0.9	1.75 – 3 2.5	1.96, 2.39, 2.8
BSO:Mn	3.68	0.82	1.45 - 3.27	1.67, 2.15, 2.6, 2.98
BSO:Fe	2.32	8.0	1.8 - 3.2	2.02, 2.75,
BSO:Cu	2.32	8.0	1.43 - 3.2	2.05, 2.63, 3.08
BSO:Mo	6,85	0.85	0.93 - 3.15	1.08, 1.81, 2.06, 2.45, 2.79. 3.15
BSO:Ag	4.25	0.87	0.88 - 2.74	0.98, 1.18, 2,56, 2.7

^{*} The components of the spectra $\Delta \alpha^{\text{phE}}(h \nu)$ with $h\nu_{\text{max}}$ are indicated by arrows in Fig. 3a and 3b.

The data in Table 2 show that doping BSO crystals significantly alters the spectral ranges and spectral positions of the intense photo absorption bands. Doping with Cr, Mn, Mo, and Cu ions improves the Ψ and K characteristics, while doping with Sn and Fe ions leads to their reduction compared to undoped BSO.

4. Conclusions

The spectral characteristics of the photochromic effect (PhE) and the induced photoconductivity (PhI) effect have been studied in undoped and doped BSO crystals. The dependences of these effects on the type of dopant and temperature have been revealed.

In BSO crystals doped with 3d and 4d transition metal ions, the PhE effect results from changes in the ratio of concentrations of the same ions in different charge states. These changes occur due to photochemical reactions triggered by photoexcitation. The impurities create deep localized centers within the BSO crystal lattice, and there is no direct link between the PhE and the photoinduced photoconductivity (PhI) effects.

In BSO crystals doped with non-transition metal ions that create acceptor levels, as well as in undoped BSO containing both donor and acceptor levels, the PhE is mainly attributed to charge redistribution between these levels. In this case, a partial correlation between the PhE and PhI effects is observed.

The intensity of the photoinduced photoconductivity (PhI) is primarily determined by the occupation of energy levels located near the edges of the conduction and valence bands. The transport of photoexcited charge carriers occurs under conditions of either fast or slow recombination, depending on the nature of these levels.

The results obtained may be applied in the development of models for deep centers in wide-bandgap semiconductors (the bandgap width of BSO crystals is 3.4 eV at 80 K). Furthermore, the findings enable a comparative analysis of the effects of various impurities on the PhE and PhI, which may promote the use of doped BSO crystals in devices for optical information processing, recording, and storage.

Acknowledgments and funding. This study was supported by the Ministry of Education and Science of Ukraine [research projects No. 0123U101854 and No. 0124U000524], the Operational Program OP JAK [Project No. CZ.02.01.01/00/22_008/0004596], and partially by the Czech Science Foundation [project No. 23-05578S].

Conflict of Interest. The authors have no conflicts to disclose.

References

- 1. Günter, P., Huignard, J.-P. Photorefractive Materials and Their Applications: Part 1 (2006). Springer: New York.
- Günter, P., Huignard, J. Photorefractive Materials and Their Applications: Parts 2 & 3 (2007). Springer: New York.
- 3. Mallick, S., Miteva, M., & Nikolova, L. (1997). Polarization properties of self-diffraction in sillenite crystals: reflection volume gratings. *Journal of the Optical Society of America B*, 14(5), 1179-1186.
- 4. Gesualdi, M. R. D. R., Barbosa, E. A., & Muramatsu, M. (2006). Advances in phase-stepping real-time holography using photorefractive sillenite crystals. *Journal of Optoelectronics and Advanced Materials*, 8(4), 1574.
- Montemezzani, G., & Zgonik, M. (1997). Light diffraction at mixed phase and absorption gratings in anisotropic media for arbitrary geometries. *Physical Review E*, 55(1), 1035.
- 6. Khromov, A. L., Kamshilin, A. A., & Petrov, M. P. (1990). Photochromic and photorefractive gratings induced by pulsed excitation in BSO crystals. *Optics Communications*, 77(2-3), 139-143.
- Lima, A. F. D., Farias, S. A. D. S., & Lalic, M. V. (2011). Structural, electronic, optical, and magneto-optical
 properties of Bi₁₂MO₂₀ (M= Ti, Ge, Si) sillenite crystals from first principles calculations. *Journal of Applied Physics*, 110(8).

- Panchenko, T. V., & Kopylova, S. Y. (2005). Photochromic properties of the doped Bi₁₂SiO₂₀ crystals. Ferroelectrics, 322(1), 69-74.
- 9. Briat, B., Reyhers, H. J., Hamri, A., Romanov, N. G., Launay, J. C., & Ramaz, F. (1995). Magnetic circular dichroism and the optical detection of magnetic resonance for the Bi antisite defect in Bi₁₂GeO₂₀. *Journal of Physics: Condensed Matter*, 7(34), 6951.
- Panchenko, T.V., Dyachenko, A.A. (2015). Excitation and erasure of photochromic effect in Bi₁₂SiO₂₀ crystals doped with Al, Ga and Sn. *Ukrainian Journal of Physical Optics*, 16, 127–133.
- Marinova, V., Veleva, M., Petrova, D., Kourmoulis, I. M., Papazoglou, D. G., Apostolidis, A. G., Vanidhis, E. D. & Deliolanis, N. C. (2001). Optical properties of Bi₁₂SiO₂₀ single crystals doped with 4d and 5d transition elements. *Journal of Applied Physics*, 89(5), 2686-2689.
- 12. Nechitailov, A., Krasinkova, M., Mokrushina, E., Petrov, A., Kartenko, N., Prokofiev, V. (2000). Impurity defects in Cr-doped Bi₁₂SiO₂₀ and Bi₁₂TiO₂₀. *Inorg. Mater. 36*, 820–825.
- 13. Żmija, J., & Małachowski, M. (2008). Photochromic effects in sillenite single crystals. *Archives of Materials Science and Engineering*, 33(2), 101-106.
- 14. Petkova, P., Vasilev, P., Mustafa, M., & Parushev, I. (2015). Vanadium States in Doped Bi₁₂SiO₂₀. *Materials Science*, 21(2), 167-172.
- 15. Ramaz, F., Rakitina, L., Gospodinov, M., & Briat, B. (2005). Photorefractive and photochromic properties of ruthenium-doped Bi12SiO20. *Optical Materials*. 27(10), 1547-1559.
- Egorisheva, A., Burkov, V., Kargin, Yu., Vasiliev, A., Volkov, V., Skorikov, V. (2001). Spectroscopic characteristics of Bi₁₂SiO₂₀ and Bi₁₂TiO₂₀ crystals doped with Mn, Mn/P, Cr/P, Cr/Ga and Cr/Cu. *Inorg. Mater. 37*, 965–973.
- Panchenko, T. V., & Strelets, K. Y. (2008). Photochromism in Cu-and Ag-doped Bi₁₂SiO₂₀ crystals. Physics of the Solid State, 50(10), 1900-1907.
- Panchenko, T.V., Strelets, K.Yu. (2009). Photochromic effect in Bi₁₂SiO₂₀ crystals doped with molybdenum. *Physics of the Solid State, 51*, 292–297.
- 19. Panchenko, T. V., Osetsky, Y. G., & Truseyeva, N. A. (1996). Photo-and electrochromic effects in Fe-and Cudoped Bi₁₂SiO₂₀ crystals. In *Ferroelectrics* (pp. 61-70).
- 20. Panchenko, T. V. (1998). Induced impurity photoconductivity in crystals of Si-and Ge-sillenites. *Physics of the Solid State*, 40(6), 938-940.
- 21. Grachev, A. I. (1999). Holographic recording in photorefractive crystals with nonstationary and nonlinear photoconductivity. *Physics of the Solid State*, 41(6), 922-927.
- 22. Kamshilin, A. A., Kobozev, O. V., Grachev, A. I., & Karavaev, P. M. (2002). Manifestation of long-lived photosensitivity gratings in two-wave mixing experiments with sillenite crystals. *Journal of the Optical Society of America B*, 19(2), 202-207.
- Siebenhofer, M., Viernstein, A., Morgenbesser, M., Fleig, J., & Kubicek, M. (2021). Photoinduced electronic and ionic effects in strontium titanate. *Materials Advances*, 2(23), 7583-7619.
- 24. Aldrich, R. E., Hou, S. L., & Harvill, M. L. (1971). Electrical and optical properties of Bi₁₂SiO₂₀. *Journal of Applied Physics*, 42(1), 493-494.
- Briat, B., Panchenko, T. V., Rjeily, H. B., & Hamri, A. (1998). Optical and magneto-optical characterization of the Al acceptor levels in Bi₁₂SiO₂₀. Journal of the Optical Society of America B, 15(7), 2147-2153.
- 26. Panchenko, T. V., Dyachenko, A. A., & Khmelenko, O. V. (2016). Photoluminescence of Bi₁₂SiO₂₀ crystals. *Ukrainian Journal of Physical Optics*, *17*(1), 39-45.
- 27. Panchenko, T. V., & Truseyeva, N. A. (1991). Optical absorption and photochromic effect in Cr and Mn doped Bi₁₂SiO₂₀ single crystals. *Ferroelectrics*, *115*(1), 73-80.
- 28. Panchenko, T. V., & Truseyeva, N. A. (1996, January). Photochromism of Bi₁₂SiO₂₀ crystals doped with transition-metal ions of Fe group. In *Tenth Feofilov Symposium on Spectroscopy of Crystals Activated by Rare-Earth and Transitional-Metal Ions* (Vol. 2706, pp. 83-92). SPIE.
- 29. Tanabe, Y., & Sugano, S. (1954). On the absorption spectra of complex ions II. *Journal of the Physical Society of Japan*, 9(5), 766-779.
- 30. Grabmaier, B. C., & Oberschmid, R. (1986). Properties of Pure and Doped Bi₁₂GeO₂₀ and Bi₁₂SiO₂₀ Crystals. *Physica Status Solidi* (a), 96(1), 199-210.
- 31. Lever, A. B.P. (1984). Inorganic Electronic Spectroscopy. Elsevier: Amsterdam.
- 32. Solé, J., Bausa, L., & Jaque, D. (2005). *An introduction to the optical spectroscopy of inorganic solids*. John Wiley & Sons.
- 33. Wardzyński, W., Baran, M., & Szymczak, H. (1981). Electron paramagnetic resonance of Fe3+ in bismuth germanium oxide single crystals. *Physica B+ C*, 111(1), 47-50.

- 34. Panchenko T.V., Trubitsyn M. P. (2023). Thermally induced effects in the optical absorption of pure and doped Bi₁₂SiO₂₀ single crystals. *Ukrainian Journal of Physical Optics*, 24(4), 04001 04007.
- Panchenko, T. V., Yanchuk, Z. Z. (1996). Photoelectric properties of crystals Bi₁₂SiO₂₀. Physics of the Solid State 38, 1113–1118.
- 36. Panchenko, T. V., Yanchuk, Z. Z. (1996). Photoconductivity of doped Bi₁₂SiO₂₀ crystals. *Physics of the Solid State* 38, 3042–3046.

Panchenko, T. V., Trubitsyn, M. P., Laguta, V. (2026). Photochromism of Doped $Bi_{12}SiO_{20}$ Crystals. *Ukrainian Journal of Physical Optics*, 27(1), 01001–01015. doi: 10.3116/16091833/Ukr.J.Phys.Opt.2026.01001

Анотація. У спектральному діапазоні 0,5–3,5 eV досліджено стаціонарне та фотоіндуковане оптичне поглинання, а також стаціонарну та фотоіндуковану фотопровідність у монокристалах $Bi_{12}SiO_{20}$, легованих іонами неперехідних Al, Ga, Sn) і перехідних металів (Fe, Cr, Cu, Mn, V, Ag, Mo). Показано, що іони перехідних металів створюють глибокі локалізовані центри. При цьому фотохромний ефект визначається внутрішньоцентровими переходами в тих іонах, концентрація яких збільшується внаслідок фотохімічних реакцій. У кристалах з іонами неперехідних металів фотохромний ефект залежить від розподілу носіїв заряду по локальних рівнях забороненої зони, структура яких змінена цими іонами. В обох випадках фотоіндукована фотопровідність визначається, в основному, зміною розподілу рекомбінаційних потоків носіїв заряду між центрами швидкої та повільної рекомбінації. Аналізується можливість взаємозв'язку між фотохромним ефектом і фотоіндукованою фотопровідністю.

Ключові слова: леговані кристали $Bi_{12}SiO_{20}$, спектри поглинання, фотохромний ефект, індукована фотопровідність